LCLS-II-HE Undulator Vacuum Chamber Heating Estimates

Heinz-Dieter Nuhn[a]

[a]SLAC National Accelerator Laboratory, Stanford University, CA 94309-0210, USA

1. INTRODUCTION

The SLAC National Accelerator Laboratory is in the process of constructing the LCLS-II/LCLS-II-HE high power x-ray free electron lasers (X-ray FELs). See Fig. 1 and Fig. 2 for the Undulator Hall cell layouts for the two projects. The final project goal includes transporting a 250 kW electron beam through the small-bore undulator vacuum chambers, which will be heated in the process. Vacuum chamber heating is an undesired side affect and needs to be mitigated. Two heating sources have been identified: (1) interaction of the electrons with their own wakefields and (2) absorption of spontaneous x-ray synchrotron radiation produced in the interaction of the electrons with the undulator magnetic fields. The contributions from these two sources will be discussed in the next two sections. If the vacuum chamber temperature is allowed to rise, it will cause an undulator gap dependent temperature increase of the permanent magnet blocks of the undulator, and thus will reduce their temperature-dependent remnant magnetic fields. The biggest concern is that a temperature gradient between the permanent magnet blocks and the support structure, which is kept at a fixed temperature by the HVAC system of the Undulator Hall, will form, causing a temperature gradient within the permanent magnet blocks, which would make it impossible to accurately predict their remnant fields and thus the undulator K values. In this document, the total power, deposited in the vacuum chamber, is estimated to help the design of a cooling system for the vacuum chamber.

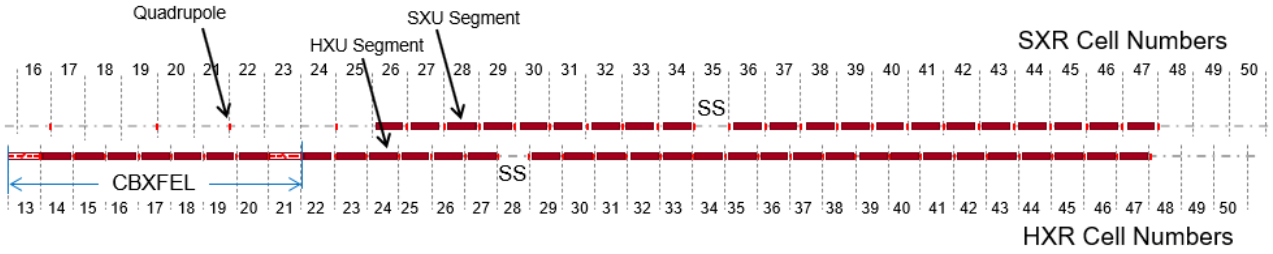

Figure 1: LCLS-II Undulator Hall cell layout.

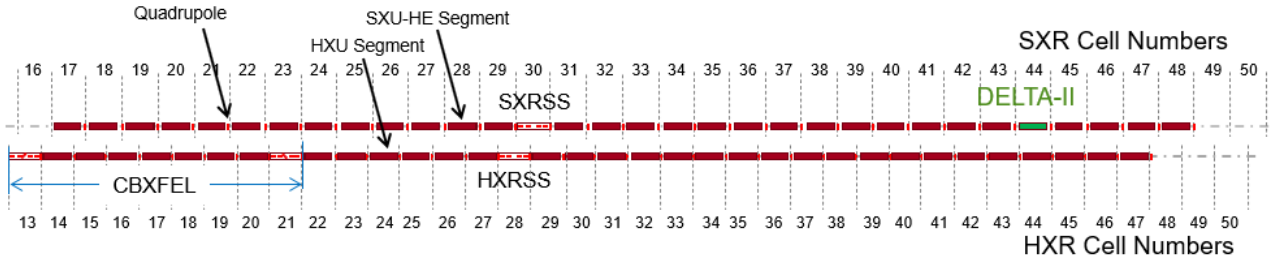

Figure 2: LCLS-II-HE Undulator Hall cell layout.

2. WAKEFIELD LOSSES

The wakefield calculations used in this document are based on a paper by K. Bane and G. Stupakov [1]. Relative induced voltage (relative beam energy loss) due to resistive wall and roughness wakefields, $\delta_w(s)$, as function of the position within the bunch, s, for a flat LCLS-II undulator vacuum chamber are shown in that paper in FIG. 6 for reference parameters: energy $E_r = 4$ GeV, undulator vacuum chamber length, $L_r = 130$ m, peak current, $I_r = 1$ kA,

Further author information: E-mail: nuhn@slac.stanford.edu

and roughness slopes 0 mrad, 15 mrad, 30 mrad and 45 mrad. The roughness slopes of the LCLS undulator vacuum chambers are, in general 20 mrad following the requirement document [2]. The LCLS-II-HE project will be adding 9 undulator vacuum chambers at the upstream end of the SXR undulator line (in cells 17-25, see Fig. 2) for which they are allowing a roughness slope of 30 mrad according to [3]. Bane and Stupakov also provide relative induced voltages for two special beam charge distributions, based on beam transport simulation results, in FIG. 7 in their paper. The relative induced voltages for those two cases are not too far off from the case of the flat-top charge distribution that we will be using in this document.

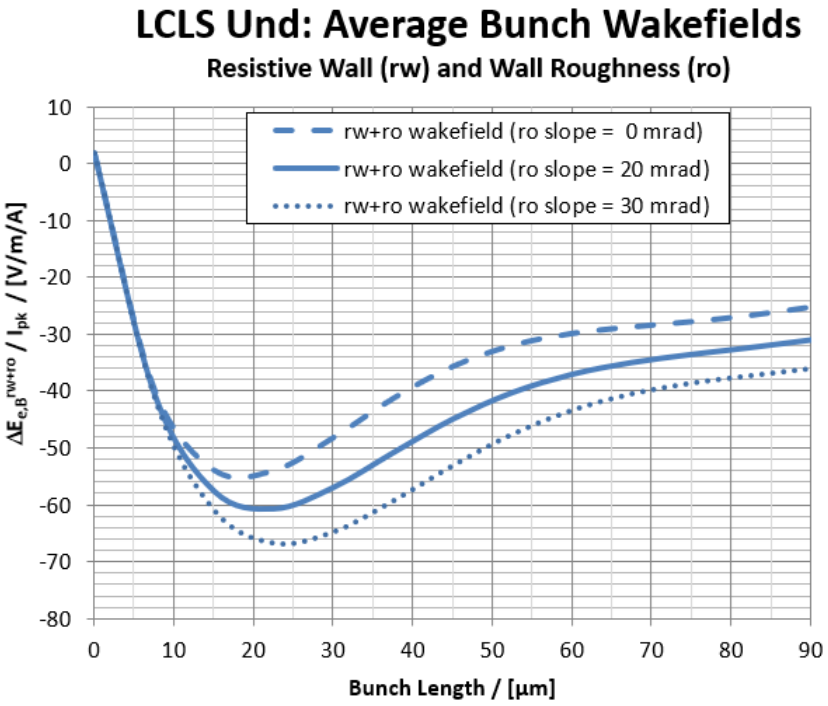

Figure 3: $\Delta E_{e,B}^{rw+ro}/\left(e\ I_{pk}\right)$ (see Eq. 3): resistive wall and roughness wakefields averaged over a bunch.

For an arbitrary peak current, I_{pk}, the relative energy loss per electron at location s within the bunch can be scaled and converted to absolute energy loss per meter travelled at location s within the bunch based on Eq. 11 in the Bane paper [1]

$$\Delta E_e^{rw+ro}\left(s\right) = I_{pk}\frac{E_r}{I_r L_r}\delta_w\left(s\right). \tag{1}$$

Note: $\Delta E_e^{rw+ro}\left(s\right)$ is independent of electron beam energy.

We calculate the average energy loss per meter traveled in a bunch of length

$$l_B = c\ Q_B/I_{pk}, \tag{2}$$

by

$$\Delta E_{e,B}^{rw+ro}\left(l_B\right) = \frac{1}{l_B}\int_0^{l_B}\Delta E_e^{rw+ro}\left(s\right)ds, \tag{3}$$

using the total bunch charge, Q_B, and the speed of light in vacuum, c. This function, normalized by I_{pk} and based on the 0 mrad and 30 mrad curves from FIG.6 in [1] and on an interpolation for 20 mrad, is shown in Fig. 3.

The total wakefield power deposited in the vacuum chamber per unit chamber length is

$$\frac{dP^{rw+ro}}{dz} = -\frac{\Delta E_{e,B}^{rw+ro}\left(l_B\right)}{e}\ \langle I\rangle\,, \tag{4}$$

i.e., the negative of the voltage lost per bunch electron times the average bunch current,

$$\langle I\rangle = f_{rep} Q_B, \tag{5}$$

with f_{rep} being the bunch repetition frequency or the number of bunches per second and e the electric charge of the electron. The term $\Delta E_{e,B}^{rw+ro}\left(l_B\right)$, makes dP^{rw+ro}/dz in Eq. 4 explicitly dependent on bunch length, which can be written, by combining Eq. 5 and Eq. 2, as $l_B = c\ \langle I\rangle / \left(I_{pk}\ f_{rep}\right)$. This makes it apparent that dP^{rw+ro}/dz is a function of I_{pk}, $\langle I\rangle$ and f_{rep}. The average beam current for both, the LCLS-II and LCLS-II-HE beams, is limited to

$$\langle I\rangle_{max} = P_{b,max}\frac{e}{E_e} \tag{6}$$

by the fact that the electron beam dumps (EBDs) can only handle beam powers up to $P_{b,max} = 120$ kW [4], which gives the maximum allowed bunch charge as function of f_{rep} and E_e

$$Q_{B,max} = \frac{e\ P_{beam,max}}{E_e\ f_{rep}}. \tag{7}$$

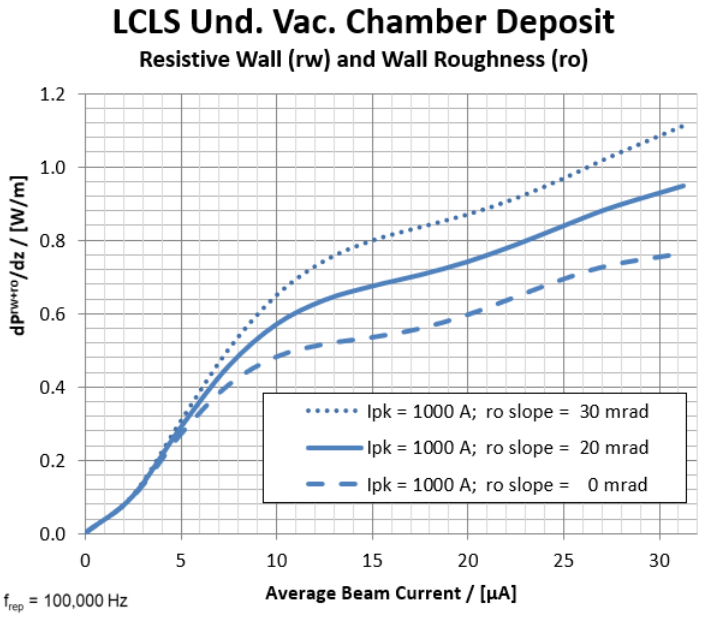

Figure 4: Power per unit distance deposited in the undulator vacuum chamber from a combination of resistive wall and roughness wakefields as function of average beam current for a beam repetition rate of 100,000 Hz according to Eq. 4.

$P_{beam,max}$ was originally planned to be upgraded to 250 kW by the LCLS-II-HE project [5]. Recently, that upgrade was cancelled [6]. Tab. 1 summarizes a number of power and bunch charge related limits for LCLS-II and LCLS-II-HE operations. The total wakfield power deposited in the vacuum chamber can now be calculated by multiplying the average bunch wakefield shown in Fig. 3 by I_{pk} and $\langle I\rangle$.

Fig, 4 shows resistive wall and roughness wakefield power deposition (through Eq. 4 using the data shown in Fig. 3) at a beam repetition rate of 0.1 MHz, the highest rate at which a bunch charge of 300 pC (for LCLS-II) is possible.

For beam repetition rates between 0.1 MHz and 1 MHz, the bunch charge needs to be reduced according to Eq. 7 by changing the bunch length according to Eq. 2, which causes the maximum power deposition to no longer be

Table 1: Operational charge limits for LCLS-II and LCLS-II-HE.

System	$P_{b,max}$ (kW)	$E_{e,max}/e$ (GeV)	f_{rep} (MHz)	$Q_{B,max}$ (pC)	$\langle I \rangle_{max}$ (μA)
LCLS-II	120	4.0	0.1	300	30
LCLS-II	120	4.0	1.0	30	30
LCLS-II-HE	120	8.0	0.1	150	15
LCLS-II-HE	120	8.0	1.0	15	15

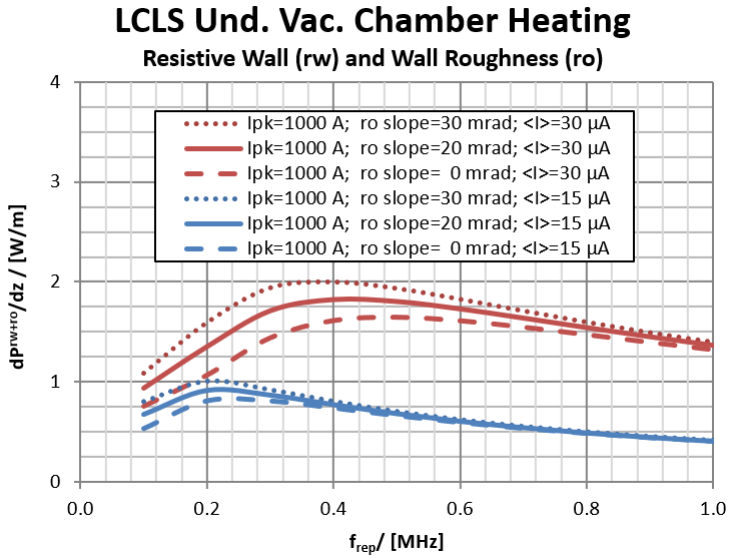

Figure 5: Power per unit distance deposited in the undulator vacuum chamber from resistive wall and roughness wakefields for different roughness slopes and maximum average beam currents as function of the bunch repetition rate according to Eq. 4.

proportional to beam repetition rate. Instead, it is determined by the functions shown in Fig. 3 and follows the curve shown in Fig. 5, which shows that, because of the limitations discussed above, the maximum wakefield power deposition in the undulator vacuum chamber peaks for LCLS-II at about 0.4 MHz with a value of 1.82 W/m, and for LCLS-II-HE at about 0.23 MHz with a value of 0.93 W/m and 1.0 W/m for the nine vacuum chambers upstream of the SXR line for LCLS-II-HE. These calculations assume a peak current of 1000 A, the maximum estimated value for beam operation. The limitation comes from the fact that the electron beam has to travel through a long (>2 km) bypass line before reaching the Undulator Hall. Wakefields generated in that bypass line will destroy beam quality for higher peak currents. Should a method be found to allow for higher peak currents in the future, the plots shown above would need to be scaled with the ratio of the achieved peak current to the value of 1000 A used to generate these plots. For a conservative approach, a safety factor of 2 should be considered, putting the expected maximum power deposited from wakefields to 3.7 W/m (LCLS-II), 1.9 W/m (LCLS-II-HE) and 2.0 W/m (in the new 9 vacuum chambers at the upstream end of the SXR line).

3. SYNCHROTRON RADIATION

As the electrons travel through the undulators, they emit synchrotron radiation in addition to the desired FEL radiation. The total amount of synchrotron radiation only depends on electron energy and undulator magnetic field but not on the details of the electron distribution within the bunches [7]

$$P_T^{sr} = \frac{N_p}{6} Z_0 \langle I \rangle \; e \frac{2\pi\, c}{\lambda_u} \gamma^2 K^2. \tag{8}$$

Here, N_p is the number of undulator periods passed, $Z_0 = \mu_0\, c \approx 377\,\Omega$ is the vacuum impedance, $\mu_0 = 4\pi \times 10^{-7}$ H/m is the vacuum permeability, λ_u is the undulator period length, $\gamma = E_e/m_e c^2$ is the relativistic Lorentz factor, $m_e c^2$

Table 2: Maximum total synchrotron radiation power levels for LCLS

System	Beamline	N_p	γ_{max}	λ_u (m)	K_{max}	$\langle I \rangle_{max}$ (A)	P_T^{sr} (W)
LCLS-II	HXR	4160	7828	0.026	2.6	0.000030	38
LCLS-II-HE	HXR	4160	15656	0.026	2.6	0.000015	75
LCLS-II	SXR	1827	7828	0.039	5.6	0.000030	138
LCLS-II-HE	SXR-HE	1800	15656	0.056	9.2	0.000015	190

is the rest energy of the electron, $K = \lambda_u e\, B_0/\left(2\pi m_e c\right) = \left(\lambda_u/2\pi\right) B_0 c/\left(m_e c^2/e\right)$ is the undulator constant and B_0 is the peak on-axis magnetic field in the undulator.

A large fraction of the synchrotron radiation power listed in the last column of Tab. 2 will travel along the beam axis without interacting with the undulator vacuum chamber. Only the radiation at large angles to the beam axis will hit the vacuum chamber, where some of it will get reflected, some will pass through, and the rest will be absorbed and will contribute to vacuum chamber heating. As a conservative approach, we assume here that half the total power will be absorbed by the vacuum chamber. As a simplification, we also assume that the absorption will occur equally along the beam path

$$\frac{dP^{sr}}{dz} = \frac{1}{2}\frac{P_T^{sr}}{L_{Und}}. \tag{9}$$

Table 3: Conservative estimate of the synchrotron radiation absorbed by the undulator vacuum chamber

System	Beamline	L_{Und} (m)	dP^{sr}/dz (W/m)
LCLS-II	HXR	127.8	0.15
LCLS-II-HE	HXR	127.8	0.29
LCLS-II	SXR	91.4	0.76
LCLS-II-HE	SXR-HE	131	0.72

4. SUMMARY

In this document, we estimate power deposition into the LCLS undulator line vacuum chambers due to wakefields and spontaneous synchrotron radiation for high power LCLS-II and LCLS-II-HE operation. Tab. 4 summarizes the estimates by listing wakefield, synchrotron radiation and total power depositions per unit chamber length.

Table 4: Conservative summary of estimates for the maximum power deposited in the undulator vacuum chamber from wakefields and synchrotron radiation. We ignore the extra wakefield heating in the first 9 LCLS-II-HE vacuum chambers, here, because the synchrotron radiation heating is reduced in the initial undulators and the reduction compensates for that slightly increased wakefield power.

System	Beamline	dP^{rw+ro}/dz (W/m)	dP^{sr}/dz (W/m)	dP^{total}/dz (W/m)
LCLS-II	HXR	3.7	0.15	3.9
LCLS-II-HE	HXR	1.9	0.29	2.2
LCLS-II	SXR	3.7	0.76	4.5
LCLS-II-HE	SXR-HE	1.9	0.72	2.7

References

[1] K. Bane and G. Stupakov, "Roughness Tolerance Studies for the Undulator Beam Pipe Chamber of LCLS-II," May 2014. LCLS-II TN-14-06.

[2] H.-D. Nuhn, "LCLS-II Undulator System Physics Requirent Document," 15 June 2017. LCLSII-3.2-PR-0038-R3.

[3] D. Cesar, "LCLS-II-HE SXR Undulator System," 19 May 2022. LCLSII-HE-1.3-PR-0049-R2.

[4] J. Galayda, "Linac Coherent Light Source II Project Requirements Document," 2 December 2015. LCLSII-1.1-GR-0018-R1.

[5] T. Raubenheimer, "Linac Coherent Light Source II High Energy Project Requirements Document," 19 April 2021. LCLSII-HE-GR-0023-R3.

[6] D. Fritz, "Electron Dump Average Beam Power Limit," August 2022. LCLSII-HE-1.1-PM-0489.

[7] K.-J. Kim, "Characteristics of Synchrotron Radiation," January 2001. X-Ray Data Booklet, LBNL/PUB-490 Rev. 2.